Int. J. Heat Mass Transfer. Vol. 14, pp. 1115–1134. Pergamon Press 1971. Printed in Great Britain

FORCED CONVECTION HEAT TRANSFER TO WATER WITH AIR INJECTION IN A RECTANGULAR DUCT

B. W. MARTIN

Department of Mechanical Engineering and Engineering Production, University of Wales, Institute of Science and Technology, Cardiff, Wales

and

G. E. SIMS

Department of Mechanical Engineering, University of Manitoba, Winnipeg, Manitoba, Canada

(*Received* 21 *July* 1970 *and in revised form* 28 *October* 1970)

Abstract—A study was made of forced convection heat-transfer to water and air–water mixtures in a horizontal rectangular duct with air injection through one porous heated wall. The main independent variables are the rate of air injection through the porous wall, the superficial liquid velocity in the duct, and the amount of air mixed with the water upstream of the heated test section; the method of mixing the upstream air and water is also varied. The dependent variables reported are the heat-transfer coefficient, over a range of approximately 60:1, and the flow pattern, extending from bubble flow through to annular flow.

The conditions analyzed are those for which the heat-transfer coefficient increases with increasing rate of air injection though the porous heat-transfer surface (analogous in saturated nucleate boiling to the heat-transfer coefficient increasing with vapour formation rate, i.e. with heat flux). For these conditions, the heat-transfer coefficients are correlated using the concept (analogous to Chen's [19] for forced convection saturated boiling) that the heat-transfer coefficient comprises two contributions, one associated with the forced convection flow and one with the bubbling at the heat-transfer surface.

NOMENCLATURE

A_T, total cross-sectional area of channel, $A_T = ab$ [ft^2];

a, height of channel normal to heated surface [ft];

b, width of channel and of heated surface [ft];

d, diameter of circular tube [ft];

d_e, equivalent diameter of flow channel,

$$d_e \equiv \frac{4(\text{cross-sectional area})}{\text{wetted perimeter}} \text{ [ft]};$$

F, upstream turbulence factor;

g, acceleration due to gravity [ft/h^2];

g_0, constant in Newton's Second Law of Motion, $4{\cdot}17 \times 10^8$ lb ft/lbf h^2;

k, thermal conductivity [Btu/fth degF];

K_T^*, dimensionless group used in correlating barbotage data, defined in equation (9);

L, length of porous heater [ft];

Nu_{bub}^*, special form of Nusselt number, defined in equation (8);

Pr, Prandtl number;

Q, volumetric flow rate [ft^3/h];

Re_f, Reynolds number for liquid phase; $Re_f \equiv \rho_f u_f d_e/\mu_f$

T, temperature [°F];

u, superficial velocity [ft/h] or [ft/s];

u_f, superficial liquid velocity in the channel, $u_f \equiv Q_f/A_T$ [ft/h] or [ft/s];

$u_{g,i}$, superficial gas velocity in the channel at entry to the heated porous section,

$$u_{g,i} \equiv \frac{Q_{g,i}}{A_T} \text{ [ft/h] or [ft/s]};$$

$\dot{V}_g''$, barbotage rate or gas volume injected through porous heater per unit time and unit heater area, [ft^3/ft^{2}h] or [ft^3/ft^{2}s];

x, position along heater [ft].

Greek symbols

α, heat transfer coefficient [Btu/ft^{2}h degF];

$\bar{\alpha}$, mean heat-transfer coefficient [Btu/ft^{2}h degF];

β, volumetric quality;

$$\beta \equiv \frac{Q_g}{Q_g + Q_f} = \frac{u_g}{u_g + u_f} = \frac{u_g/u_f}{u_g/u_f + 1};$$

μ, dynamic viscosity [lb/ft h];

ρ, density [lb/ft^3];

σ, surface tension [lbf/ft];

Ψ, bubble effectiveness factor;

Ψ_0, bubble effectiveness factor for zero-inlet-quality tests;

Ψ^+, ratio Ψ/Ψ_0.

Subscripts

B, bulk conditions;

bub, maximum obtainable due to bubbling for fixed fluid properties and bubbling rate;

cr, critical;

f, liquid;

g, gas;

i, conditions at inlet to the heated porous section;

mac, due to macroconvection

meas, measured;

mic, due to microconvection;

0, refers to tests with zero inlet quality;

pred, predicted;

SP, single phase;

T, total cross-section;

TP, two phase, but restricted to conditions of zero barbotage and finite inlet quality.

INTRODUCTION

BOILING is a very important method of heat transfer, particularly in systems, such as nuclear reactors and liquid propellant rocket motors, which involve high heat-flux densities. However, boiling is a complex phenomenon affected by many variables. Several authors [1–9] have therefore sought to improve the understanding of heat transfer across bubble-stirred boundary layers by simulating nucleate boiling using "barbotage" or electrolysis to produce bubbles on the heat-transfer surface. (The term "barbotage" is here defined as the bubbling of a gas through a drilled or porous heat-transfer surface into a liquid.) Barbotage systems are attractive for the study of bubble-stirred boundary layers mainly because, in contrast with boiling, the bubble generation rate is independent of the rate of heat transfer and can be accurately controlled and measured [10]. The study of barbotage systems then, by contributing to the understanding of bubble-stirred boundary layers, should ultimately improve the knowledge of boiling systems, thus resulting in improved boiling heat-transfer correlations.

Previous forced convection heat-transfer investigations of barbotage in enclosed channels are due to Gose *et al.* [1, 2] and Kudirka *et al.* [6], all in vertical round tubes with upward flow of the liquid or gas–liquid mixtures. The latter were nitrogen–water [1], air–water [2, 6] and air–ethylene glycol [2, 6], with provision for mixing gas upstream of the heated porous test section in [6]. Collectively, these researchers covered a range of Reynolds numbers from 380 to 50,000 and barbotage rates up to 0·62 ft/s.

Gose *et al.* [2] observed that the effect of barbotage was approximately "linearly additive" to the effect of single-phase forced convection, i.e. for a given barbotage rate and liquid, the absolute increase in the heat-transfer coefficient over that for single-phase flow was approximately the same regardless of the value of the heat-transfer coefficient in the absence of barbotage. Kudirka *et al.* [6] found that the effect of barbotage was "algebraically additive", i.e. the magnitude of the effect of barbotage on the heat-transfer coefficient depended not only on the barbotage rate and the liquid, but also on the factors affecting the heat-transfer coefficient in the absence of barbotage (superficial liquid velocity and gas velocity along the channel).

The present experiments are of forced convection barbotage for water and air–water mixtures flowing in a horizontal rectangular duct having a bottom porous heated wall through which air is bubbled and transparent side-walls for flow pattern observation. This geometry, for which no barbotage measurements have previously been reported, simulates that of a rocket motor cooling channel; the present research forms part of a larger investigation [11–13] of this geometry which also involves real boiling.

The main dependent variables are the heat-transfer coefficient and the flow pattern; the main independent variables are the barbotage rate $\dot{V}_g''$ (rate of air injection through the porous heating surface), the superficial water velocity in the channel u_f, and the superficial air velocity in the channel upstream of the heated porous test section $u_{g,i}$. A minor independent variable is the method of introducing the air into the water upstream of the test section. Interest centres on conditions where the heat-transfer coefficient increases with barbotage rate $\dot{V}_g''$ (analogous in boiling to the increase in the heat-transfer coefficient with vapour formation rate, i.e. with heat flux).

APPARATUS AND PROCEDURE

Only the essentials of the apparatus are described below; a more detailed account may be found in [14]. The test section (shown in Fig. 1) consists of a horizontal rectangular channel of internal cross-sectional dimensions 0·52 × 0·257 in. (equivalent diameter 0·344 in.) with the 0·52 in. side vertical. In the bottom of the channel for a length of 5·91 in. is a heated porous element 0·0365-in. thick and 0·257-in. wide through which air is bubbled. The method of sealing between the porous element and the sides of the channel is shown in Fig. 1. The heated porous section is preceded by a 6-in. length and followed by an observation section of 12-in. length of the same cross-section. The sides of the channel are of transparent plastic $\frac{3}{8}$-in. thick.

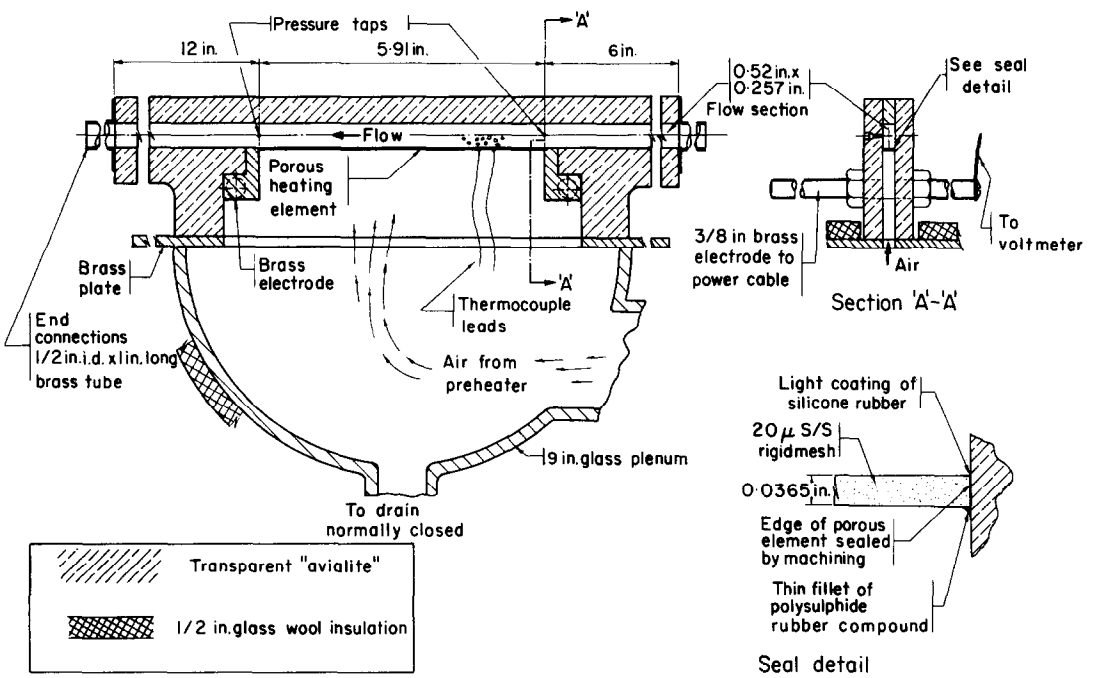

FIG. 1. Diagram of test section.

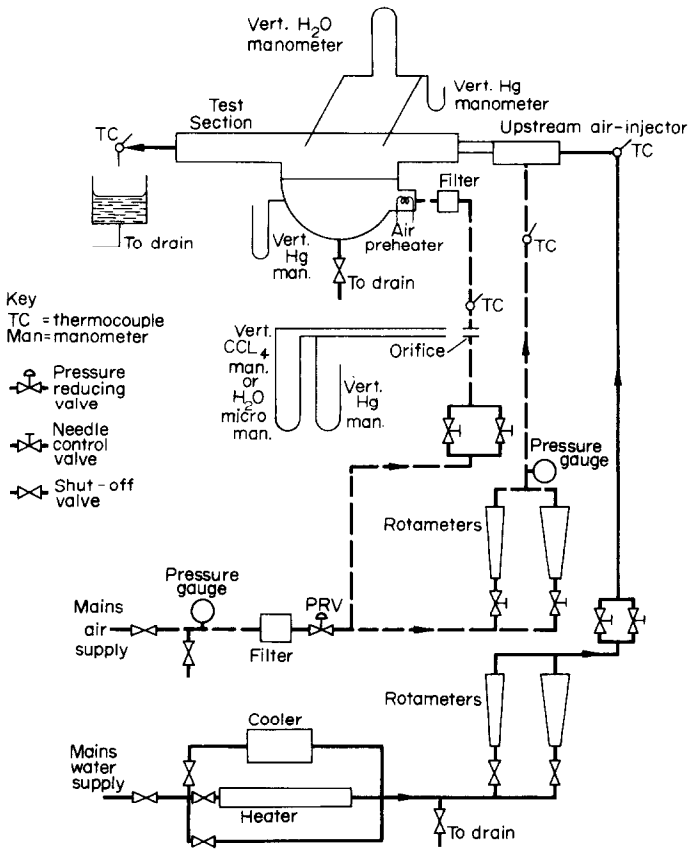

FIG. 2. Flow diagram.

The porous element consists of stainless steel "Rigid Mesh" of 20 μ nominal pore size, chosen for its suitability as a resistance heater in terms of electrical resistivity, availability in thin sections, good strength and ready machinability. The rms surface roughness is approximately 0·0006 in. in the direction along the channel; other details may be found in [14]. Electrical resistance heating was preferred on account of simplicity, minimum external heat losses and time to reach thermal equilibrium. A constant voltage transformer was used to ensure a steady ac supply of 240 V (±1 per cent) with a variable autotransformer for control and calibrated ammeter and voltmeter for measurement.

Two types of thermocouple were electrically resistance-welded along the bottom centre-line of the porous element at approximately 1-in. intervals. One type was iron–constantan (Honeywell Controls Ltd., 30 B. & S. gauge, type J), while the other was copper–constantan (Honeywell Controls Ltd., 30 B. & S. gauge, type T). A thermocouple from each reel of wire was calibrated in a bath over the temperature range used in the present experiments. Separate cold junctions were used and thermocouple emf's were read on a Tinsley type 4025 precision potentiometer.

The water circuit, air-to-test-section circuit and air-to-upstream-injector circuit are all shown in Fig. 2. As a precaution, all thermocouples shown were individually calibrated, those measuring water temperature being isolated from any electrical contact with the water. Water flow rates were measured by calibrated rotameters. Air supplied at 56 psig under steady

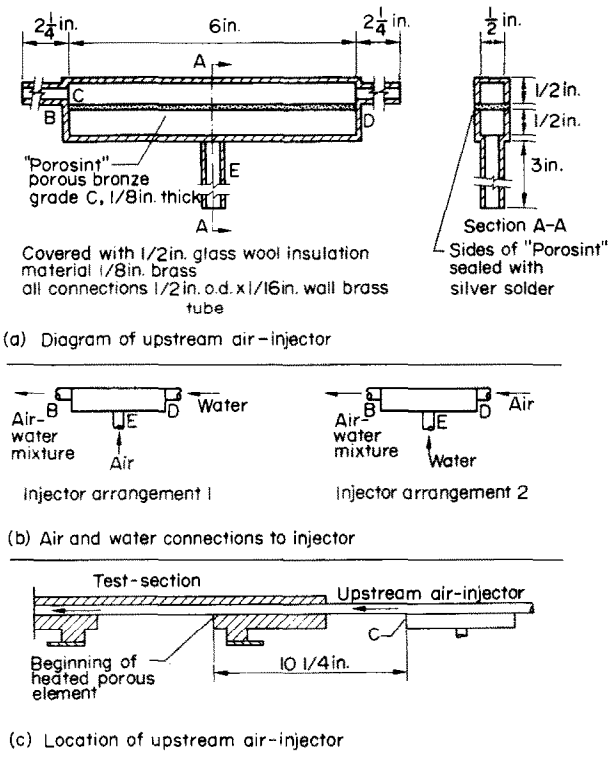

FIG. 3. Upstream air-injector.

conditions to the test section was measured by calibrated orifice, the pressure drop being measured on either a vertical U-tube carbon tetrachloride manometer or a water micro-manometer depending on the air flow rate. The air flow rate to the upstream injector was measured using calibrated rotameters.

A diagram of the upstream air-injector used to introduce the air into the water upstream of the heated test section is shown in Fig. 3a. The air and water were introduced in one of two arrangements depicted in Fig. 3b. In the first, the air was introduced into the water through the porous material on the bottom of the injector (connection E), while the water entered the horizontal connection D, the mixture leaving through the horizontal outlet connection B. In the second arrangement, the inlet water and air connections were reversed. For both arrangements, the position of the injector with respect to the test section was the same (Fig. 3c). These arrangements represented two entirely different methods of introducing upstream air into the water, with the object of determining the effect on the heat-transfer coefficient. The injector was located sufficiently far upstream of the test section to ensure (i) thermal equilibrium* at the beginning of the heated element (confirmatory tests are described in [14]), and that (ii) over the length of the test section the flow patterns were stable.

High-speed still photographs of the flow patterns in the channel were taken with a 5 × 4 M.P.P. camera and a microflash light-source of 5μs duration and 12 joules energy. The light source was mounted behind the test section with a diffusing screen placed between the light

* "Thermal equilibrium" here means that the temperature of both phases was equal and the air was saturated with water vapour at the prevailing temperature.

source and the test section. Stroboscobic flow-observations were also made.

A first series of tests was conducted with zero air flow to the upstream injector, where water only was present at inlet to the heated porous section ($u_{g,i} = 0$). This condition is termed "zero inlet quality"*; the analogous condition in a boiling experiment is when water at its saturation temperature is supplied to a heated test section. For a given run, the superficial water velocity u_f was held constant and the barbotage rate $\dot{V}_g''$ varied from the largest values to zero (single-phase liquid flow). Subsequent tests, in which some air was supplied to the upstream injector, so giving an air–water mixture at entry to the heated porous section ($u_{g,i}$ finite), are called "finite inlet quality" tests. In each test, the superficial water velocity u_f and barbotage rate $\dot{V}_g''$ were held constant while the superficial air velocity $u_{g,i}$ at inlet to the heated porous section was increased in steps from zero. The equilibrium condition for all tests was that readings did not change over a period of 10 min.

Repeatability checks were made throughout the program; the rms repeatability was 5·4 per cent. In all tests the water inlet temperature was approximately 68°F, with about 10°F temperature difference between heating surface and bulk water. The inlet pressure to the heated section ranged between 14·8 and 21·6 psia. It should be noted that subcooled boiling could not occur under these conditions as the heating surface temperature was at least 130 degF below the saturation temperature. The estimated error [14] in u_f is 2·5 per cent and in $u_{g,i}$ is 3·2 per cent, while for by far the majority of the data, the error in the heat-transfer coefficient is 10 per cent or less and in $\dot{V}_g''$ is 3·7 per cent.

FLOW PATTERN OBSERVATIONS

Although there is as yet no completely standard nomenclature in describing flow patterns in horizontal two-phase flow, the terminology of Alves [15] (and of Baker [16]) has been used by a number of investigators and wherever possible, will be followed herein. Because Alves' flow patterns refer to flow in a channel where there is no gas injection through the channel walls, they require modification to describe patterns when gas is injected through one of the channel walls in the section under observation. Even without gas injection through the channel walls, two patterns not specifically described by Alves will be used here (froth and stratified froth flow). The flow pattern boundaries are, of course, not sharply defined; there is a gradual transition from one pattern to another.

For zero-inlet-quality tests, the term "two-phase boundary layer" will be used to describe the layer within which the gas and liquid mixture is contained and which grows from the beginning of the porous section.

The salient features of each flow pattern are described below and are illustrated in Fig. 4. For a given pattern, e.g. bubble flow, more than

Table 1. Flow patterns and boundaries for zero-barbotage, finite-inlet-quality tests

Superficial liquid velocity u_f(ft/s)	Injector arrangement	Flow pattern	Sketch in Fig. 4	Approximate boundary upstream injection rate $u_{g,i}$(ft/s)
0·29	1	Stratified	d(ii)	
		Slug	e	1·9
		Annular	f	28
1·55	1	Bubble	a(iii)	
		Stratified	d(i)	1·2
		froth		3·7
		Slug	e	
		Annular	f	20
		Plug	b	
	2	Slug	e	4·5
		Annular	f	19
5·1	1	Bubble	a(iv)	
		Froth	c(vii)	4·3
		Slug	e	6·1
		Annular	f	14

* It is understood that neither $u_{g,i}$ nor $u_{g,i}/u_f$ are synonymous with inlet quality. The relation is given in the Nomenclature.

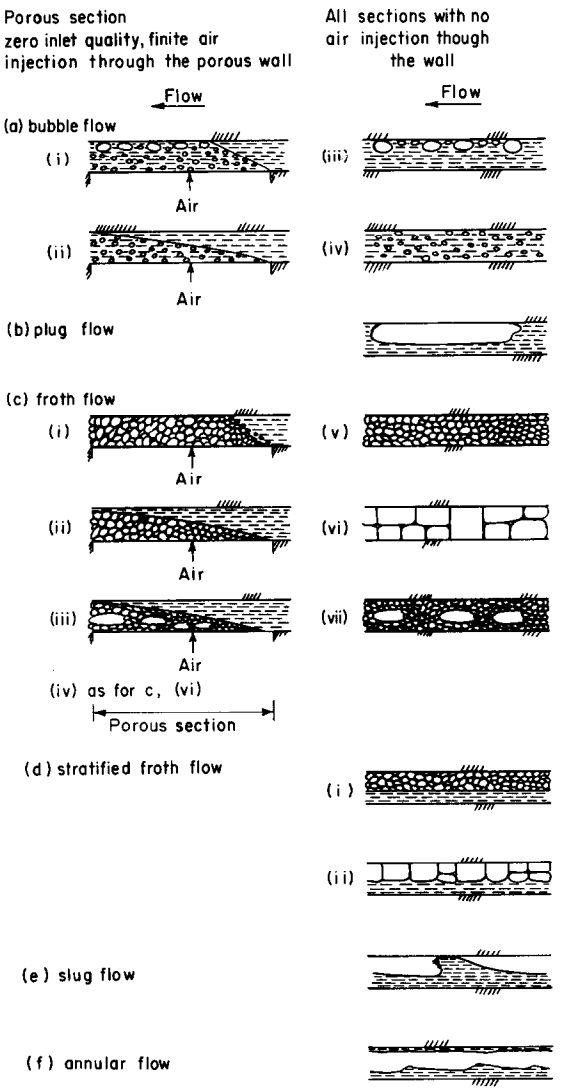

FIG. 4. Flow pattern sketches.

one sketch may appear depicting the different conditions encountered within that pattern; each sketch is referred to either on the flow-map in Figure 5 or in Table 1, as follows:

(a) *Bubble flow.* The main characteristic is the existence of spherical or nearly-spherical discrete bubbles.

(b) *Plug flow.* Long bubbles of a bullet shape, occupying about 2/3 of the channel height, travel along the top of the channel separated by plugs of liquid.

(c) *Froth flow.* The main feature of this flow is coalescence; bubbles touch each other and coalesce, resulting in a "frothy" mixture which is either contained within the "two-phase boundary layer" or fills the channel. In the "froth" the liquid is the continuous phase, but is transported mainly in the form of the film between the bubbles or air cells. Included within this flow pattern is the condition where coalescence results in a bullet-shaped bubble approximately $\frac{3}{4}$-in. long which travels down the centre-line of the channel.

(d) *Stratified froth flow.* A layer of liquid flows along the bottom of the channel covered by a frothy layer extending to the top of the channel.

(e) *Slug flow.* A wave of water periodically seals the top of the channel and passes along the channel.

(f) *Annular flow.* The liquid flows in a film around the inside wall of the channel and the air flows as a central core; large amplitude waves may still form on the bottom film of water, but the crest of the wave does not appear to seal the channel.

Flow patterns in the porous section for zero-inlet-quality tests

For $u_{g,i} = 0$ and finite $\dot{V}''_g$ the two main flow patterns observed in the porous section are bubble flow and froth flow. Figure 5 shows the boundary between these two regions and indicates the relevant flow pattern sketch. For the two highest superficial liquid velocities tested ($u_f = 3{\cdot}1$ and $5{\cdot}1$ ft/s) the two-phase boundary layer does not touch the top of the channel within the porous section [e.g. Fig. 4c (ii)] while for the other superficial liquid velocities tested ($u_f \leqslant 1{\cdot}55$ ft/s) it does [e.g. Fig. 4c (i)].

Only three other investigations are known to the authors where flow patterns have been observed or inferred in a channel with gas addition through the walls of the section of interest; these are by Wallis and Griffith [17], Wallis [10] and Kudirka *et al.* [6]. In none of these works was the channel geometry that of

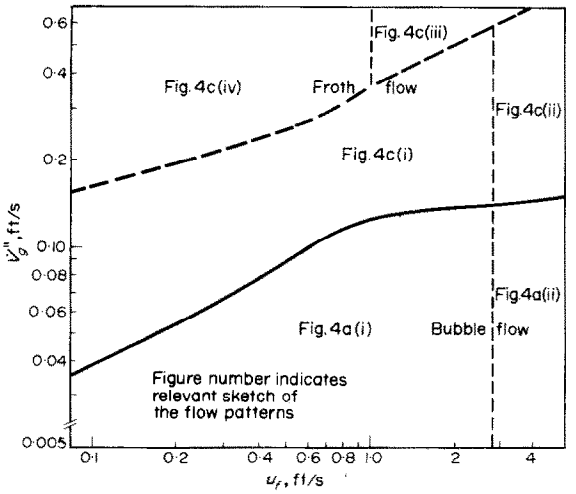

FIG. 5. Flow patterns in the porous section for zero-inlet-quality tests.

the present investigation. As with the Wallis and Griffith [17] experiment, there is no significant change in flow pattern along the length of the porous section. A detailed comparison between the present and the Wallis and Griffith flow pattern observations is available in [14].

Observations of flow patterns were also made in the outlet section of the channel. It was noted that under some conditions the flow pattern is different in the outlet section compared with the porous section. The most significant difference is that under some conditions slug flow exists in the outlet section while froth flow exists in the porous section. Wallis [10] has made a similar observation with horizontal tubes. Some caution must therefore be exercised in inferring flow patterns in a bubbling section from observations made downstream of the bubbling section.

Flow patterns for zero barbotage and finite inlet quality

The flow patterns observed for $\dot{V}_g'' = 0$ and finite $u_{g,i}$ are listed in Table 1 together with the approximate $u_{g,i}$ at the pattern boundaries and the figure number of the relevant flow pattern sketch. In the present experiments, at $u_f =$ 1·55 ft/s both arrangements of the upstream injector were used to determine whether the method of mixing of the phases upstream would affect the heat-transfer coefficient in the test section; at low values of $u_{g,i}$ a marked difference in flow pattern was noted with the two injector arrangements used. With Injector Arrangement 1, in order of increasing $u_{g,i}$, the patterns observed are bubble, stratified froth, slug, and annular flow, while with Injector Arrangement 2, plug flow is observed in place of bubble and stratified froth flow. (This last difference markedly affects the heat-transfer coefficient.) The transition to slug flow is only mildly affected by injector arrangement, (transitions at $u_{g,i} \simeq 3{\cdot}7$ and 4·5 ft/s for Injector Arrangements 1 and 2 respectively) while there is virtually no effect on the slug-to-annular flow boundary ($u_{g,i} \simeq$ 20 ft/s).

In the present zero-barbotage experiments, from approximately 3 in. from the inlet connection (9 equivalent diameters) to the outlet connection (a further 21 in. or 60 equivalent diameters downstream), there is no significant change in flow pattern.

In [14] a comparison is made between the flow patterns observed here and those observed in some of the better-known works with impermeable-walled tubes. The conclusion drawn is that there is, in detail, disagreement among the various investigators as regards the flow patterns which are occurring and the position of the boundaries (not a new conclusion); the worst discrepancies occur at low values of $u_{g,i}$, where, at least in the present work, the flow pattern is affected by the method of mixing the two phases. There is however, broadly speaking, general agreement among the present and other investigators in the occurrence of the slug and annular flow patterns.

Flow pattern observations with finite barbotage and finite inlet quality

The pattern observed in the inlet section before the porous section is that described for zero barbotage and finite inlet quality and tends in general to persist throughout the porous section (Wallis [10] has made a similar observa-

tion in horizontal porous tubes) with the following modifications or exceptions.

(i) For inlet stratified froth or bubble flow, the pattern becomes froth flow in the porous section for $\dot{V}_g''$ greater than approximately 0·1 ft/s.

(ii) For inlet plug, slug, or annular flow, in the porous section the liquid on the bottom of the channel becomes either interspersed with bubbles or froth.

PRESENTATION AND DISCUSSION OF HEAT-TRANSFER MEASUREMENTS

The mean heat-transfer coefficient $\bar{\alpha}$, used in the present work, is defined as:

$$\bar{\alpha} \equiv \frac{1}{L}\int_0^L \alpha \, dx, \qquad (1)$$

where L is the total length of the heated porous test section, α is the local heat-transfer coefficient and x is position along the heater. The $\alpha \sim x$ relation is obtained by connecting linearly the local (α, x) points; the lines connecting the two (α, x) points closest to each end of the heater are extrapolated to the ends of the heater. Details of the calculation of α are given in [14]. Mean heat-transfer coefficients are therefore discussed below; the "bar" above α is omitted while α still retains the significance of a mean.

The reliability of present results for $\dot{V}_g'' = 0$ and $u_{g,i} = 0$ (single-phase liquid) may be assessed by comparison with the correlation of James *et al.* [13]; these authors obtained a correlation within ± 10 per cent of their own measured mean heat-transfer coefficients in rectangular ducts heated on one side, i.e. as for the present geometry. The present data lie satisfactorily within $+10$ and -15 per cent of this correlation.

Tests with zero inlet quality

Measurements* for the zero-inlet-quality tests are presented in Fig. 6. The symbol α_0 is used for the heat-transfer coefficient under conditions of zero inlet quality. In Fig. 6, for a fixed barbotage rate $\dot{V}_g''$ the heat-transfer coefficient α_0 generally increases with increasing u_f, a trend also observed by Gose *et al.* [1, 2] in vertical porous tubes. For a given u_f, the $\alpha_0 \sim \dot{V}_g''$ curve at first rises steeply with increasing $\dot{V}_g''$; the curves then pass through a "knee" beyond which the in-

* Tabulated data for all the heat-transfer measurements are available from the authors.

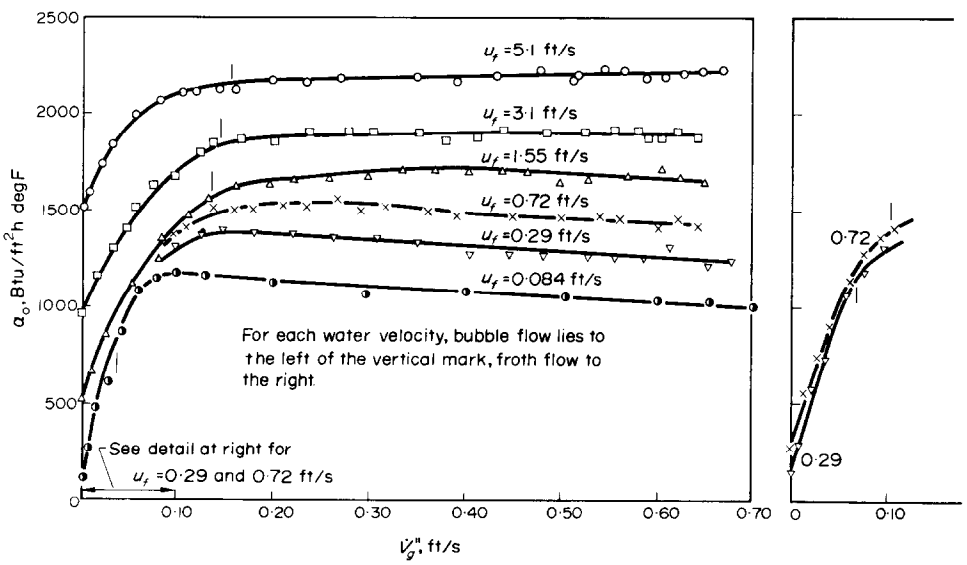

FIG. 6. Heat-transfer coefficients for zero-inlet-quality tests.

crease in α_0 with $\dot{V}_g''$ is markedly reduced. Except at the highest u_f, the curves then exhibit a maximum beyond which α_0 decreases with an increase in $\dot{V}_g''$. The boundary between bubble flow and froth flow is marked (short vertical lines); the region of steeply rising α_0 corresponds approximately with bubble flow. As in free convection [4, 18], the value of $\dot{V}_g''$ at which a maximum occurs in a plot of α or $\alpha_0 \sim \dot{V}_g''$ for a constant inlet quality is called the "critical" barbotage rate $\dot{V}_{g,\mathrm{cr}}''$. For $u_f \leqslant 1{\cdot}55$ ft/s the maximum in any $\alpha_0 \sim \dot{V}_g''$ curve is easily seen while for $u_f = 3{\cdot}1$ ft/s the maximum is vague and the way in which the smoothed curve has been drawn may not be fully justified. For $u_f = 5{\cdot}1$ ft/s, the highest liquid velocity used in the present experiments, no maximum in α_0 occurred within the range of $\dot{V}_g''$ tested.

Tests with finite inlet quality

Measurements for tests with zero barbotage and finite inlet quality are shown in Fig. 7; the symbol α_{TP} is used for the heat-transfer coefficient under these conditions ($\dot{V}_g'' = 0$, finite $u_{g,i}$). Here α_{TP} increases with u_f for given $u_{g,i}$. An important feature in Fig. 7 is that with Injector Arrangement 1, α_{TP} does not increase monotonically with $u_{g,i}$ and appears to be a function of the flow pattern. For superficial liquid velocities u_f of 1·55 and 0·29 ft/s and for increasing $u_{g,i}$, α_{TP} shows a steep increase in stratified froth flow. With the onset of slug flow α_{TP} begins to decrease; the curve exhibits a minimum and then increases as slug flow fully develops and progresses into annular flow. At the highest superficial liquid velocity of 5·1 ft/s there is no stratified froth flow. Froth flow occurs where stratified froth flow would otherwise be expected to occur; slug flow occurs over a small range of $u_{g,i}$. For this velocity there is no region of steeply increasing or decreasing α_{TP} with increasing $u_{g,i}$ which, therefore, appears characteristic only of stratified froth flow followed by slug flow.

Tests performed at a superficial water velocity of 1·55 ft/s with Injector Arrangement 2 are also shown in Fig. 7. With this arrangement α_{TP} increases monotonically with $u_{g,i}$, to give at low values of $u_{g,i}$ (by contrast with Injector Arrangement 1) plug flow, lower values of α_{TP} and a smoothly increasing α_{TP} with increasing $u_{g,i}$. In well-developed slug flow and annular flow, both injector arrangements give the same heat-transfer coefficients. The heat-transfer coeffi-

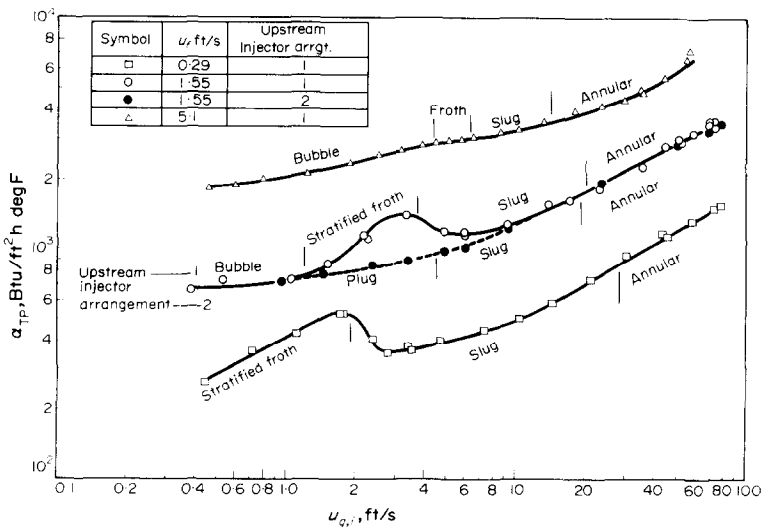

FIG. 7. Heat-transfer coefficients for tests with zero barbotage and finite inlet quality.

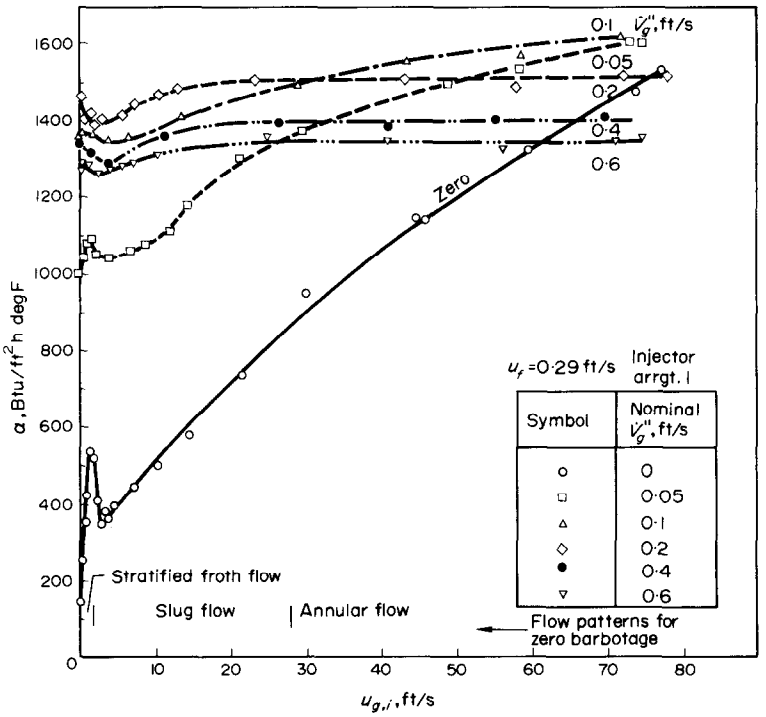

FIG. 8. Heat-transfer coefficients for finite-inlet-quality tests.
(a) u_f = 0·29 ft/s.

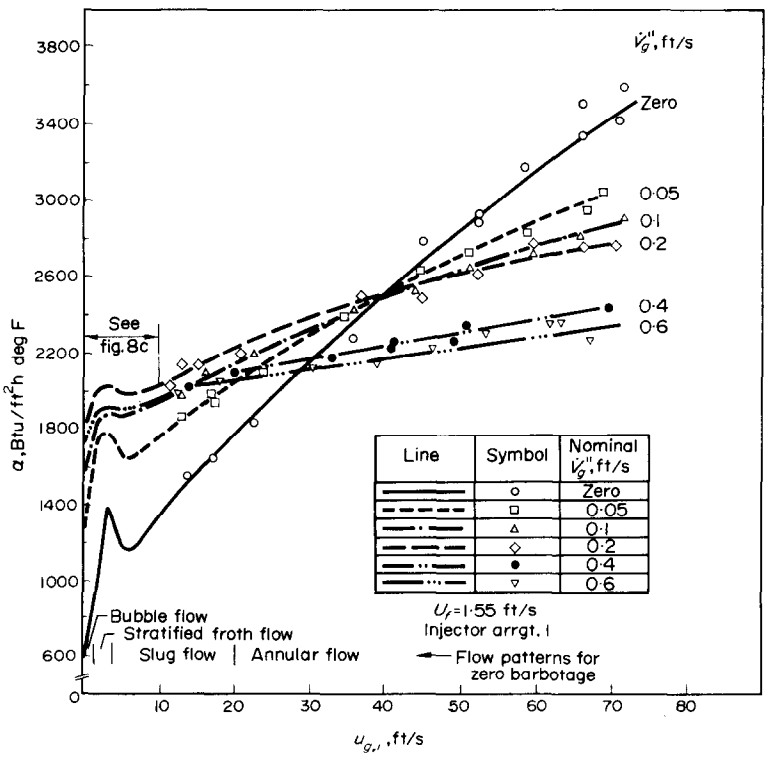

(b) u_f = 1·55 ft/s, complete range of $u_{g,i}$.

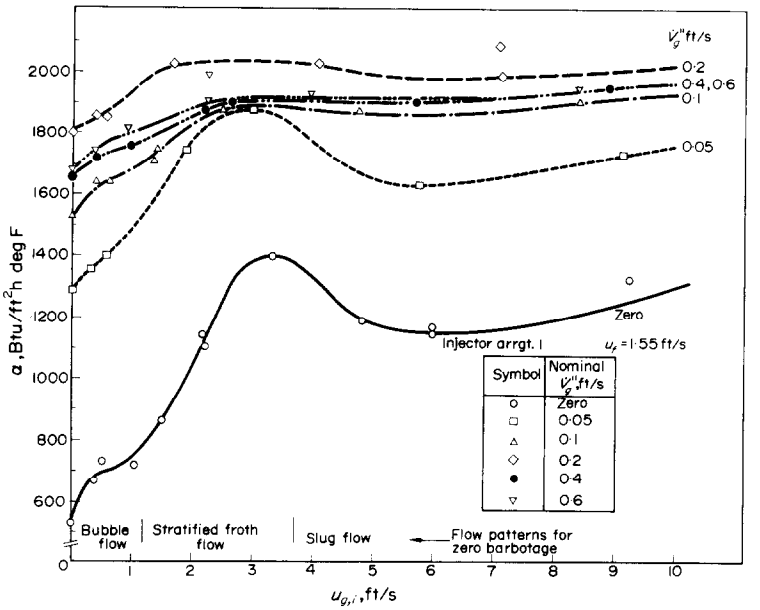

(c) $u_f = 1{\cdot}55$ ft/s, $u_{g,i} < 10$ ft/s.

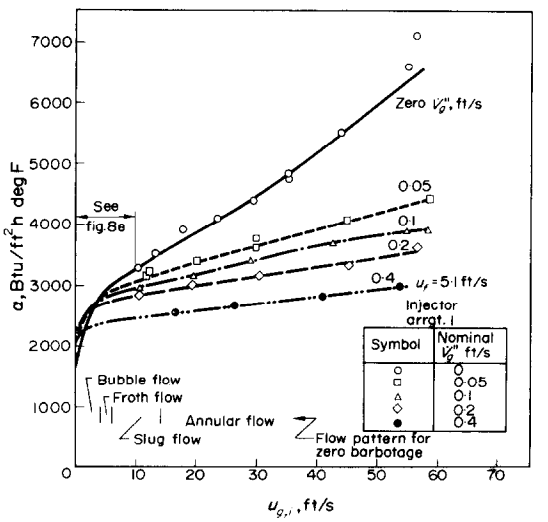

(d) $u_f = 5{\cdot}1$ ft/s, complete range of $u_{g,i}$.

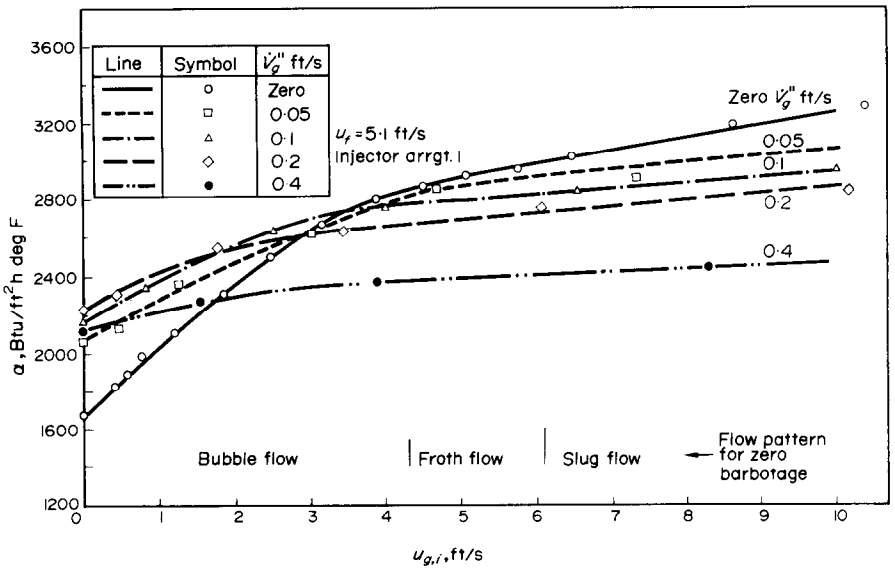

(e) $u_f = 5{\cdot}1$ ft/s, $u_{g,i} < 10$ ft/s.

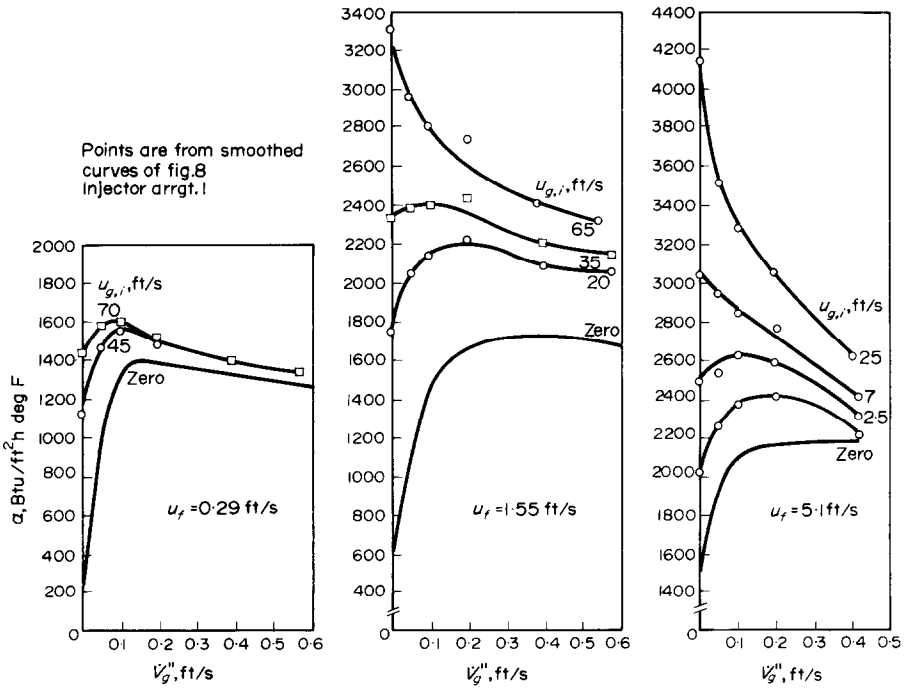

FIG. 9. Heat-transfer coefficients for finite-inlet-quality tests.

cient thus depends on the flow pattern. Where more than one flow pattern can exist, not only gas and liquid flow rates, but also the flow pattern, need to be specified.

Results of tests with finite V_g'' and finite $u_{g,i}$ are shown in Figs. 8 and 9. Figure 8a is for $u_f = 0{\cdot}29$ ft/s; the results for $u_f = 1{\cdot}55$ ft/s are shown in Fig. 8b for the complete range of $u_{g,i}$ covered while Fig. 8c shows in greater detail the range for $u_{g,i} < 10$ ft/s. Similarly, for $u_f = 5{\cdot}1$ ft/s, Fig. 8d shows the complete range of $u_{g,i}$ covered while Fig. 8e presents the data for $u_{g,i} < 10$ ft/s. Figure 9 is a cross-plot of the smoothed data contained in Fig. 8. All the data shown in these figures are for Injector Arrangement 1. The flow patterns for zero-barbotage tests are marked in Fig. 8. Any changes in flow pattern in the porous section which result because of finite barbotage have been discussed above.

In Figs. 8 and 9, as $\dot{V}_g''$ increases, α becomes increasingly insensitive to $u_{g,i}$. This may be illustrated by considering, for instance, Fig. 8b for $u_f = 1{\cdot}55$ ft/s. For $\dot{V}_g'' = 0$, on increasing $u_{g,i}$ from zero to 72 ft/s, the heat-transfer coefficient increases by $5\frac{1}{2}$ times while for $\dot{V}_g'' = 0{\cdot}6$ ft/s, the increase in α is only 40 per cent over the same range of $u_{g,i}$. The trough which occurs with the zero-barbotage experiments at $u_{g,i} \simeq 2$ ft/s for $u_f = 0{\cdot}29$ ft/s and at $u_{g,i} \simeq 4$ ft/s for $u_f = 1{\cdot}55$ ft/s is considerably reduced as $\dot{V}_g''$ is increased. For $u_f = 1{\cdot}55$ ft/s and $u_{g,i} > 40$ ft/s, and for $u_f = 5{\cdot}1$ ft/s and $u_{g,i} > 4$ ft/s, there is a monotonic decrease in α with increasing $\dot{V}_g''$ for fixed $u_{g,i}$, which is best illustrated in Fig. 9.

For $u_f = 1{\cdot}55$ ft/s, tests were run with Injector Arrangement 2 at $\dot{V}_g'' = 0$ (discussed above), 0·05 and 0·6 ft/s with increasing $u_{g,i}$. For fixed values of $u_{g,i}$ the trend is the same for both injector arrangements: for $u_{g,i} < 10$ ft/s, α increases with increasing $\dot{V}_g''$ for the three $\dot{V}_g''$ values tested; for $u_{g,i} > 40$ ft/s α decreases with increasing $\dot{V}_g''$. In the region $10 < u_{g,i} < 40$ ft/s, the behavior of α undergoes a transition. Comparing the heat-transfer coefficients obtained with the two different injector arrangements at fixed values of $u_{g,i}$, agreement is generally good where both injector arrangements give the same flow pattern (annular and well-developed slug flow) while discrepancies are greatest where differences in flow patterns exist, as in Fig. 7 for $u_{g,i} < 5$ ft/s and $\dot{V}_g'' = 0$.

Correlation of forced convection heat-transfer data for barbotage rates less than the critical

As already stated, barbotage rates less than the critical ($V_g'' < V_{g,cr}''$, i.e. the region in which the heat-transfer coefficient increases with increasing barbotage rate $\dot{V}_g''$) are analogous in saturated boiling to the "nucleate" region in which the heat-transfer coefficients increase with increasing vapour formation rate, i.e. with heat flux. The following method of correlating the heat-transfer coefficient in this region is similar to that of Chen [19] for the boiling of saturated liquids in two-phase forced convective flow. Chen postulated that two basic mechanisms take part in this process. These are (i) the ordinary "macroconvective" mechanism of heat transfer which normally operates with flowing fluids, and (ii) the "microconvective" mechanism associated with bubble nucleation and growth. He further supposed that the two mechanisms are additive in their contributions to total heat transfer. For barbotage, the analogous concept of two additive contributions is used here, one for the forced convection flow (α_{mac}) and one for bubbling (α_{mic}):

$$\alpha = \alpha_{mac} + \alpha_{mic} = \alpha_{SP}F + \alpha_{bub}\Psi \qquad (2)$$

where (i) F is an "upstream turbulence factor" accounting for the increased velocity and turbulence in the forced convective flow due to air having been introduced upstream of the test section and therefore a function of $u_{g,i}/u_f$; (ii) α_{bub} is the maximum attainable heat-transfer coefficient for a given $\dot{V}_g''$ and fluid properties, due to agitation by barbotage bubbles; α_{bub} is here called the "bubbling function"; (iii) Ψ is a "bubble effectiveness factor", accounting for the reduced effectiveness of the barbotage-bubble agitation process as turbulence in the

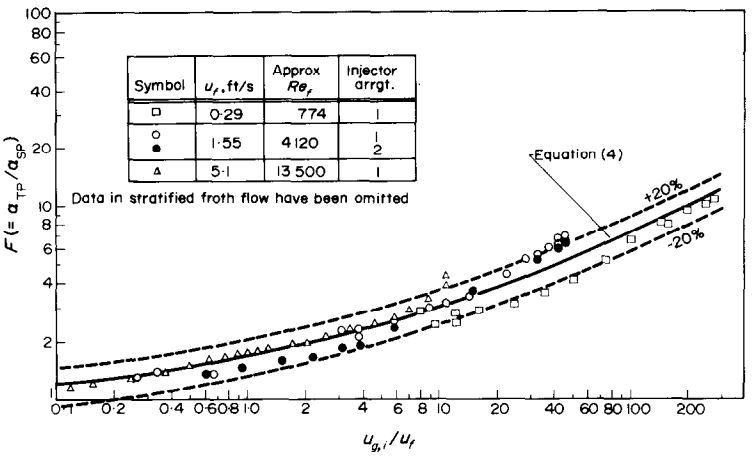

FIG. 10. Correlation of present zero-barbotage data.

forced convective flow increases, and thus a function of $u_{g,i}/u_f$ and the liquid-phase Reynolds number Re_f. The functions F, α_{bub} and Ψ remain to be determined empirically.

The F-function is found from zero-barbotage experiments, in which case $\alpha_{bub} = 0$ and equation (2) can be re-written as

$$F = \frac{\alpha}{\alpha_{SP}} = \frac{\alpha_{TP}}{\alpha_{SP}}. \tag{3}$$

When F is plotted against $u_{g,i}/u_f$ as in Fig. 10, α_{TP}/α_{SP} is practically independent of liquid velocity, the measurements being correlated by

$$F = 1 + 0{\cdot}64\sqrt{(u_{g,i}/u_f)} \tag{4}$$

such that when $u_{g,i}/u_f = 0$, $F = 1$. Except for nine data points in stratified froth flow, equation (4) correlates 88 per cent of the remaining zero-barbotage measurements to within ± 20 per cent. No meaningful comparisons can be made with existing two-phase two-component heat transfer investigations in horizontal impermeable-wall channels [20–25] all of which were in round tubes and under otherwise very different conditions.

The bubbling function α_{bub} is obtained from analysis of the zero-inlet-quality results where, since $u_{g,i}/u_f = 0$, $F = 1$ from equation (4) and $\Psi = \Psi_0 = f(Re_f)$. Equation (2) may then be re-written

$$\alpha_{bub} = \frac{\alpha_0 - \alpha_{SP}}{\Psi_0} = \frac{\alpha_0 - \alpha_{SP}}{f(Re_f)} \tag{5}$$

and hence α_{bub} may be determined from measurements of α_0 and α_{SP} together with the relationship between Ψ_0 and Re_f which best correlates α_{bub} in terms of $\dot{V}_g''$. With low mainstream turbulence, for instance in pools or laminar forced convection, Ψ_0 is virtually independent of Re_f, but as turbulence develops Ψ_0 may be expected to decrease with increasing Re_f. The simplest functional relation which collapses the zero-inlet-quality measurements as shown in the logarithmic plot of α_{bub} (for given fluid properties and porous surface) in Fig. 11 is

$$\left.\begin{aligned} \Psi_0 &= 1 && Re_f \leqslant 2000 \\ \Psi_0 &= 9{\cdot}78\, Re_f^{-0{\cdot}3} && Re_f \geqslant 2000 \end{aligned}\right\}. \tag{6}$$

The ± 15 per cent band in Fig. 11 covers all but points 1, 2 and 3 with errors in α_0 of 8, 12 and 7·5 per cent respectively.

The correlation between α_{bub} and $\dot{V}_g''$ suggested by the two full straight lines meeting at $\dot{V}_g'' = 0{\cdot}08$ ft/s in Fig. 11 may be expressed as indicated in [14] in the following dimensionless forms, fluid properties being evaluated at wall

temperature:

$$\left.\begin{aligned} Nu^*_{bub} Pr_f^{0.2} &= 167 K^{*}_{T}{}^{0.75} \quad 0.009 \leqslant K^*_T \leqslant 0.15 \\ Nu^*_{bub} Pr_f^{0.2} &= 48.7\, K^{*0.1}_T \quad 0.15 \leqslant K^*_T \leqslant 1.27 \end{aligned}\right\} \tag{7}$$

where

$$Nu^*_{bub} \equiv \frac{\alpha_{bub}}{k_f}\sqrt{\left[\frac{\sigma g_0}{g(\rho_f - \rho_g)}\right]} \tag{8}$$

$$K^*_T \equiv \frac{\dot{V}''_g \rho_f{}^{\frac{1}{2}}}{[\sigma g_0 g(\rho_f - \rho_g)]^{\frac{1}{4}}} \tag{9}$$

and the Prandtl number index is derived from the pool barbotage data of Gose *et al.* [2].

The bubble effectiveness factor Ψ for finite inlet quality is conveniently expressed in terms of Ψ_0 by

$$\Psi = \Psi^+ \Psi_0 \tag{10}$$

where Ψ^+ is correlated as a function of Re_f and $u_{g,i}/u_f$ such that, as indicated above, when the latter is zero, $\Psi^+ = 1$ and $\Psi = \Psi_0$. The relation obtained [14] for Ψ^+ from measurements is

$$\Psi^+ = \exp\left\{-\frac{0.68}{10^6}\frac{u_{g,i}}{u_f} Re_f{}^{1.4}\right\}. \tag{11}$$

Values of Ψ from equations (6), (10) and (11) have an upper limit of unity and decrease to approach zero as Re_f and $u_{g,i}/u_f$ tend to infinity, thus confirming that increased turbulence in the forced convection flow decreases the effectiveness of the bubble agitation process.

The heat-transfer coefficient as defined in equation (2) may therefore be predicted for $\dot{V}''_g < \dot{V}''_{g,cr}$ with both finite barbotage and finite upstream quality from measured α_{SP}, and F, α_{bub} and Ψ derived from the correlations in equation (4), equation (7), and equations (6), (10) and (11), respectively. Such predictions will be generally accurate over the ranges covered to within ± 15 per cent.

In making meaningful comparisons of heat-transfer coefficients in barbotage and nucleate boiling, the vapour formation rate and latent heat transport in the latter must be known [14, 26]. This is available in pool boiling, but since the necessary information is not yet available in forced convection boiling, no such comparisons have been attempted with the present

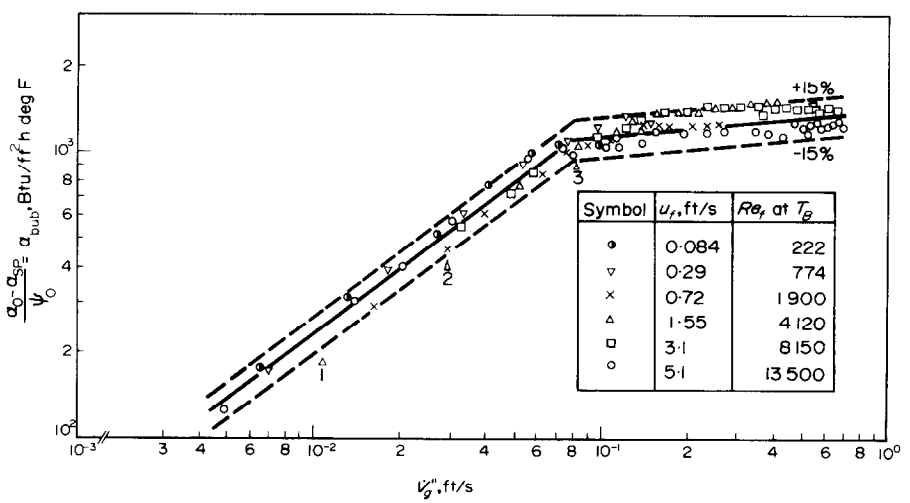

FIG. 11. Collapsed zero-inlet-quality data for $\dot{V}''_g < \dot{V}''_{g,cr}$.

forced convection barbotage research. The above correlation procedure is nevertheless that used by Chen, [19] in forced convection boiling.

Comparison of present results with other forced convection barbotage investigations

The data of Gose *et al.* [1] and of Gose *et al.* [2] are amenable to analysis in the same manner as for the present results. In both investigations, vertical porous tubes were used with zero-inlet-quality conditions; nitrogen–water in the earlier [1] and air–water and air–ethylene glycol in the latter [2] investigations were used.

Analysis shows that the Ψ_0-function found for the present results fits the results of Gose *et al.* [1] very well indeed. When the present Ψ_0-function is used in conjunction with equation (5) and their measured values of α_0 and α_{SP}, a good collapse of their data is obtained on coordinates of α_{bub} vs. $\dot{V}_g''$, or in dimensionless form, on coordinates of $Nu^*_{bub}Pr_f^{0.2}$ vs. K_T^* with fluid properties evaluated at wall temperature; only four data points out of 25 lie outside the ± 20 per cent band around the best mean line, this line being shown in Fig. 12.

The Ψ_0 function for the Gose *et al.* [2] results is found to be

$$\left.\begin{aligned} \Psi_0 &= 1 && \text{for } Re_f \leqslant 2000 \\ \Psi_0 &= 2{\cdot}14\, Re_f^{-0{\cdot}1} && \text{for } Re_f \geqslant 2000 \end{aligned}\right\} \quad (12)$$

The trends are the same as for the present Ψ_0-function, but for $Re_f > 2000$, the dependence of Ψ_0 on Re_f is considerably weaker ($Re_f^{-0{\cdot}1}$ for Gose *et al.* [2], compared with $Re_f^{-0{\cdot}3}$ for the present investigation). Indeed, on the basis of their measurements, Gose *et al.* [2] conclude that the effect of barbotage on the heat transfer is "linearly additive" to the effect of forced convection. This is the equivalent of having $\Psi_0 = 1$ in equation (5) or (12). For the largest values of Re_f ($\simeq 50000$) used by these authors, $\Psi_0 \simeq 0{\cdot}73$ from equation (12), which to a first approximation does not differ markedly from 1 (so justifying their conclusion based on their own data). However, the results of the present investigation support the observation of Kudirka *et al.* [6] that the effect of barbotage on the heat transfer is "algebraically additive" to the effect of forced convection, that is Ψ_0, and more generally, Ψ are not necessarily equal to 1.

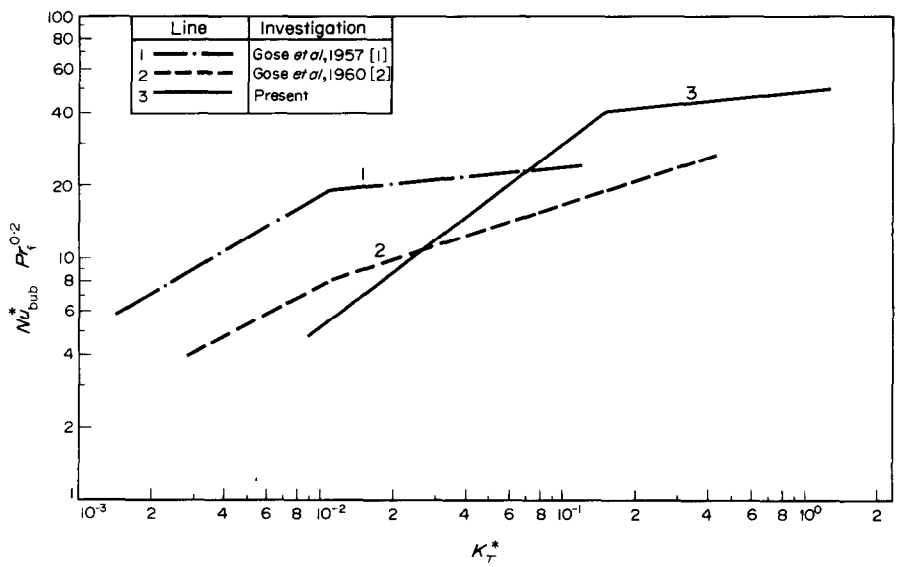

FIG. 12. Comparison of experimental dimensionless α_{bub}-functions.

Values of α_{bub} obtained from equation (5) with Ψ_0 from equation (12) were plotted [14] on dimensionless coordinates of $Nu^*_{bub}Pr_f^{0.2}$ vs. K^*_T. This form of plotting collapsed both the air–ethylene glycol and air–water data onto the same line with three of 32 data points falling outside the ± 20 per cent band of the best mean line, this line being shown on Fig. 12.

The results of the Gose *et al.* [1], Gose *et al.* [2] and the present investigations are therefore shown together in Fig. 12. All investigations show the same trends, but discrepencies among them can be large. It was indicated [2] that the Gose *et al.* [1] work was more in the nature of a preliminary investigation. The maximum discrepancy between the present and the Gose *et al.* [2] investigations occurs at $K^*_T \simeq 0{\cdot}15$ with the latter lying some 50 per cent below the former. [However, it should be borne in mind that α_0 here is obtained from

$$\alpha_0 = \alpha_{SP} + \Psi_0 \alpha_{bub}; \qquad (13)$$

errors in α_{bub}, when multiplied by Ψ_0 ($\leqslant 1$) and added to α_{SP}, produce smaller errors in α_0.] Probably some of the discrepancies among the investigations are attributable to the use of different porous surfaces as well as to the different geometry.

The data of Kudirka *et al.* [6] cannot be analyzed to give Ψ- and α_{bub}-functions. However, the present functions may be used to predict the heat-transfer coefficient α_{pred} under their experimental conditions for $\dot{V}''_g < \dot{V}''_{g,cr}$. When this exercise is performed, as in [14], the ratio of $\alpha_{meas}/\alpha_{pred}$, where α_{meas} is the measured value of the heat-transfer coefficient, lies within $+15$ and -35 per cent of the value of 1·0, which is surprisingly good. The existing discrepancies between the measured and predicted values of the heat-transfer coefficient may be attributed to the use of different porous surfaces, different geometries and the fact that the predicting equations were based on average heat-transfer coefficients while the measured heat-transfer coefficients of Kudirka *et al.* [6] were local values at one x/d position.

The present and previous barbotage experiments are analogous to boiling experiments in which either saturated liquid or a two-phase mixture is fed to the heated test section. Qualitatively at least, it should be possible to simulate subcooled boiling. This could be done in barbotage by having zero inlet quality to the heated porous section and using (with water as the liquid) a water-soluble barbotage-gas, for instance carbon dioxide. In this case the gas bubbles would dissolve in the liquid stream, similar to vapour bubbles condensing in a subcooled liquid stream.

CONCLUSIONS

1. In the present investigation of forced convection barbotage, two regimes have been distinguished, depending on inlet quality and superficial water velocity. In one regime, the heat-transfer coefficient α decreases monotonically with barbotage rate $\dot{V}''_g$ for all finite barbotage rates while in the other regime α increases with $\dot{V}''_g$, passes through a maximum at the "critical" barbotage rate $\dot{V}''_{g,cr}$, and then decreases with increasing $\dot{V}''_g$.

2. Of greater interest is the second regime, which is analogous in boiling to the increase in the heat-transfer coefficient with increasing vapour formation rate, i.e. with heat flux. The heat-transfer coefficients for this regime are correlated using the concept (analogous to Chen's [19] proposal for forced convection saturated boiling) that the heat-transfer coefficient comprises two contributions, one associated with the forced convective flow and one associated with the barbotage bubbling.

3. The present measurements support the observation of Kudirka *et al.* [6] made with a vertical porous tube that the effect of barbotage is "algebraically additive" to the effect of forced convection.

4. For the case of zero barbotage and increasing inlet quality, the behaviour of the heat-transfer coefficient depends strongly on the flow pattern.

ACKNOWLEDGEMENTS

The work described above was carried out at Imperial College of Science and Technology under the terms of a Ministry of Technology contract. The authors acknowledge the help given by the Rocket Propulsion Establishment; they are also indebted to Dr. B. W. A. Ricketson, Mr. D. G. Martin and Professor D. B. Spalding. This paper is British Crown Copyright and is reproduced by permission of the Controller of Her Britannic Majesty's Stationery Office.

REFERENCES

1. E. E. Gose, E. E. Petersen and A. Acrivos, On the rate of heat transfer in liquids with gas injection through the boundary layer, *J. Appl. Phys.* **28**, 1509 (1957).
2. E. E. Gose, A. Acrivos and E. E. Petersen, Heat transfer to liquids with gas evolution at the interface, presented at the Mexico City meeting of the A.I.Ch.E. (1960).
3. F. O. Mixon, Jr., W. Y. Chon and K. O. Beatty, Jr., The effect of electrolytic gas evolution on heat transfer, *Chem. Engng Prog. Symp. Ser.* **56**, 75–81 (1960).
4. N. U. Akturk, Heat transfer from a heated porous surface to a pool of liquid with gas injection at the interface, *Proc. of the Symposium on Two Phase Flow*, Vol. II, Exeter, pp. D 501–520 (1965).
5. P. L. Duffield, Diffusion-controlled electrolysis at a porous electrode with gas injection, Ph.D. Thesis, Dept. of Mechanical Engineering, Imperial College, University of London (1966).
6. A. A. Kudirka, R. J. Grosh and P. W. McFadden, Two-phase heat transfer in a tube with gas injection from the walls, ASME Paper No. 65-HT-47 (1965).
7. Y. Bard and E. F. Leonard, Heat transfer in simulated boiling, *Int. J. Heat Mass Transfer* **10**, 1727–1734 (1967).
8. W. J. Frea and J. H. Hamelink, Heat transfer from the wall of a porous solid involving gas injection and vaporization, *ASME Paper* No. 68-HT-46 (1968).
9. H. Beer and F. Durst, Mechanismen der Wärmeübertragung beim Blasensieden und ihre Simulation, *Chemie Ing.-Tech.* **40**, 632–638 (1968).
10. G. B. Wallis, Some hydrodynamic aspects of two-phase flow and boiling, *Proc. of the* 1961 *International Heat Transfer Conference*, Boulder, Colorado, Part II, pp. 319–340 (1961).
11. D. B. Spalding, Heat transfer to rocket motors, Inaugual Lecture, Imperial College, London, December (1958).
12. D. D. James, C. J. Bardoliwalla and D. G. Martin, An apparatus for the study of boiling heat transfer to a fluid flowing in a rectangular duct, Paper No. 11, I. Mech. E. Symposium on Two-Phase Fluid Flow, London (1962).
13. D. D. James, B. W. Martin and D. G. Martin, Forced convection heat transfer in asymmetrically heated ducts of rectangular cross-section, *Proceedings of the Third International Heat Transfer Conference*, Chicago, Vol. 1, pp. 85–98 (1966).
14. G. E. Sims, Forced convection heat transfer to water with air injection through one porous heated wall of a rectangular duct, Ph.D. Thesis, Dept. of Mechanical Engineering, Imperial College, University of London (1969).
15. G. E. Alves, Co-current liquid–gas flow in a pipe-line contactor, *Chem. Engng Prog.* **50**, 449–456 (1954).
16. O. Baker, Simultaneous flow of oil and gas, *Oil Gas J.* **53**, 185–195 (1954).
17. G. B. Wallis and P. Griffith, Liquid and gas distributors in a two-phase boiling analogy, Technical Report No. 13 DSR 7-7673, Massachusetts Institute of Technology (1958).
18. G. E. Sims, U. Akturk and K. O. Evans-Lutterodt, Simulation of pool boiling heat transfer by gas injection at the interface, *Int. J. Heat Mass Transfer* **6**, 531–535 (1963).
19. J. C. Chen, A correlation for boiling heat transfer to saturated liquids in convective flow, ASME Paper No. 63-HT-34 (1963).
20. H. A. Johnson and A. H. Abou-Sabe, Heat transfer and pressure drop for turbulent flow of air–water mixtures in a horizontal pipe, *Trans. Am. Soc. Mech. Engrs* **74**, 977–987 (1952).
21. L. Fried, Pressure drop and heat transfer for two-phase, two-component flow. *Chem. Engng Prog. Symp. Ser.* **50**, 47–51 (1954).
22. H. A. Johnson, Heat transfer for viscous-turbulent flow of oil–air mixtures in a horizontal pipe, *Trans. Am. Soc. Mech. Engrs* **77**, 1257–1264 (1955).
23. D. R. Oliver and S. J. Wright, Pressure drop and heat transfer in gas–liquid slug flow in horizontal tubes, *Br. Chem. Engng* **9**, 590–596 (1964).
24. I. H. Newson, Heat transfer and pressure drop during pipe flow of two-phase two-component mixtures, Ph.D. Thesis, Dept. of Chemical Engineering, University College, University of London (1964).
25. R. H. Pletcher and H. N. McManus, Jr., Heat transfer and pressure drop in horizontal annular two-phase, two-component flow, *Int. J. Heat Mass Transfer* **11**, 1087–1104 (1968).
26. P. L. Duffield and G. E. Sims, Comparison of heat-transfer coefficients in pool barbotage and pool boiling, Report BHT/R/1, Dept. of Mechanical Engineering, Imperial College, London (1969).

CONVECTION THERMIQUE FORCÉE DANS L'EAU AVEC INJECTION D'AIR DANS UN CONDUIT RECTANGULAIRE

Résumé—On a fait l'étude du transfert thermique par convection forcée vers de l'eau et des mélanges air–eau dans un conduit rectangulaire avec injection d'air au travers d'une paroi poreuse chauffée. Les principales variables indépendantes sont le flux d'injection d'air à travers la paroi poreuse, la vitesse pariétale du

liquide dans le conduit et la quantité d'air mélangée à l'eau en amont de la section chauffée. On fait aussi varier la méthode de mélange de l'air et de l'eau en amont. Les variables dépendantes rapportées sont les coefficients de transfert thermique sur un domaine approximatif de 60 à 1, et le type d'écoulement s'étendant de l'écoulement avec bulles à l'écoulement annulaire.

Les conditions analysées sont celles pour lesquelles le coefficient de transfert thermique croît avec le flux croissant d'air injecté à trayers la surface poreuse (analogie lors d'une ébullition nucléée saturée avec le coefficient de transfert thermique qui croît en même temps que le taux de formation de vapeur c'est-à-dire le flux thermique). Dans ces conditions les coefficients de transfert thermique sont unifiés à l'aide du concept (analogue à celui de Chem pour une ébullition saturée à convection forcée) selon lequel le coefficient de transfert thermique comprend deux contributions, l'une associée à l'écoulement à convection forcée et l'autre au bouillonnement à la surface qui transfère la chaleur.

WÄRMEÜBERGANG BEI ERZWUNGENER KONVEKTION AN WASSER IN RECHTECKKANÄLEN MIT LUFTEINBLASUNG

Zusammenfassung—Es wurde eine Studie durchgeführt über den Wärmeübergang bei erzwungener Konvektion an Wasser und Wasser-Luft-Gemische in einem rechteckigen Kanal mit Luft-Einleitung durch eine poröse, beheizte Wand. Die unabhängigen Hauptveränderlichen sind die durch die poröse Wand eingeleitete Luftmenge, die Flüssigkeitsgeschwindigkeit an der Oberfläche des Kanals und die Luftmenge im Wasserstrom vor dem beheizten Testabschnitt. Die Methode der Vermischung von Wasser und Luft wurde ebenfalls variiert. Die behandelten abhängigen Veränderlichen sind die Wärmeübergangszahl, im Bereich von annähernd 60:1, und die Gestalt der Strömung, von der Blasenströmung bis zur Ringströmung.

Für die untersuchten Bedingungen gilt, dass die Wärmeübergangszahl mit zunehmender Lufteinströmung durch die poröse, wärmeübertragende Oberfläche zunimmt (analog steigt beim gesättigten Blasensieden die Wärmeübergangszahl mit zunehmender Dampfdichte, das heisst mit zunehmendem Wärmestrom). Für diese Bedingungen wurden Wärmeübergangszahlen so in eine Beziehung gebracht (analog zu dem von Chen [19] für gesättigtes Sieden bei Zwangskonvektion), dass die Wärmeübergangszahl in zwei Teile zerfällt, in einen für die Zwangskonvektion und in einen für die Blasenbildung an der Heizfläche.

ПЕРЕНОС ТЕПЛА ПРИ ВЫНУЖДЕННОЙ КОНВЕКЦИИ К ВОДЕ В ПРЯМОУГОЛЬНОМ КАНАЛЕ С ВДУВОМ ВОЗДУХА

Аннотация—Изучался перенос тепла при вынужденной конвекции к воде или воздушно-водяным смесям в горизонтальном прямоугольном канале с вдувом воздуха через одну пористую нагретую стенку. Основными независимыми переменными являются скорость вдува через пористую стенку, скорость фильтрации жидкости в трубе и количество воздуха, смешанного с водой в верхней части нагретого рабочего участка. Изменялся также способ перемешивания верхнего воздуха и воды. Зависимыми переменными были коэффициент теплообмена в пределах 60 : 1, а также картина течения от пузырькового до кольцевого.

Анализировались условия, при которых коэффициент теплообмена увеличивается с увеличением скорости вдува воздуха через пористую поверхность теплообмена (аналогично тому, как при насыщенном пузырьковом кипении коэффициент теплообмена увеличивается со скоростью парообразования, т.е. скоростью теплового потока). Для таких условий коэффициенты теплообмена обобщаются, используя понятие (аналогично Чену [19] для насыщенного кипения при вынужденной конвекции) о том, что коэффициент теплообмена включает две составляющие: одну, связанную с вынужденным конвективным течением, и другую — с образованием пузырьков на поверхности теплообмена.